






## Article

# Tribological Performance of ZnO Green Particles as Lubricating Oil Additives

Giovanna Gautier di Confiengo <sup>1,\*</sup> , Eligio Malusà <sup>2</sup>, Massimo Guaita <sup>2</sup> , Silvia Motta <sup>2</sup> , Mattia Di Maro <sup>1</sup>   
and Maria Giulia Faga <sup>1</sup> 

<sup>1</sup> Istituto di Scienze e Tecnologie per l'Energia e la Mobilità Sostenibili (STEMS)—Sede Secondaria di Torino, Consiglio Nazionale delle Ricerche, Strada delle Cacce 73, 10135 Torino, Italy; mattia.dimaro@stems.cnr.it (M.D.M.)

<sup>2</sup> Consiglio per la Ricerca in Agricoltura e l'Analisi dell'economia Agraria—Centro di Ricerca Viticoltura ed Enologia, via P. Micca 35, 14100 Asti, Italy; eligio.malus@crea.gov.it (E.M.); massimo.guaita@crea.gov.it (M.G.)

\* Correspondence: giovanna.gautier@stems.cnr.it

**Abstract:** ZnO particles, synthesized using a green method, were used as additives to enhance the tribological properties of lubricants. Polyphenolic extracts obtained from by-products of the winemaking process from two grape varieties, Barbera (red berry) and Moscato (white berry), were utilized as reducing agents in the synthesis of ZnO starting from two Zn salts (nitrate and acetate). The grape extracts were analysed for their polyphenolic profile. The ZnO particles were characterized by X-ray diffraction, SEM, FESEM, and FTIR. A ball-on-disk tribometer was used to study the tribological behaviour of the ZnO particles as oil additives in comparison to a reference base oil. Electron microscopy (SEM) and energy dispersive spectroscopy (EDS) were used to characterise wear scars. Polyphenolic compounds were more abundant in the Moscato extracts than in the Barbera extracts. Although FTIR analyses evidenced differences in the region related to the stretching of carbonyl bonds, all kinds of ZnO particles were crystallised in their pure phase, as shown by the XRD patterns. Morphological analysis revealed that precursors significantly influenced particle size and shape, with acetate producing regular-shaped nanoparticles (50–200 nm) while nitrate produced pyramid-like particles (10–20 μm). Addition of ZnO to oil resulted in a more stable friction coefficient (COF) than the reference oil, with lower values obtained using ZnO particles obtained from acetate compared to nitrate. The addition of the ZnO particles derived from Barbera by-products lowered on average wear values compared to the pure lubricant oil.

**Keywords:** green synthesis; ZnO; lubrication additives; polyphenolic compounds; circular economy



**Citation:** Gautier di Confiengo, G.; Malusà, E.; Guaita, M.; Motta, S.; Di Maro, M.; Faga, M.G. Tribological Performance of ZnO Green Particles as Lubricating Oil Additives. *Sustainability* **2024**, *16*, 6810. <https://doi.org/10.3390/su16166810>

Academic Editor: Md. Shahinoor Islam

Received: 21 June 2024

Revised: 26 July 2024

Accepted: 2 August 2024

Published: 8 August 2024



**Copyright:** © 2024 by the authors. Licensee MDPI, Basel, Switzerland. This article is an open access article distributed under the terms and conditions of the Creative Commons Attribution (CC BY) license (<https://creativecommons.org/licenses/by/4.0/>).

## 1. Introduction

The agricultural sector produces a lot of by-products that are considered waste, which can become high-polluting material [1]. The cost associated with the treatment, storage, and transportation of these wastes is affecting the production cost of food. In the context of a circular economy and sustainable waste management, the valorization of these agri-food industrial wastes provides a very strong chance to generate new usable bioproducts [2]. Wine industry wastes, which mostly consist of solid byproducts, can account for over 30% (*w/w*) of the grapes used for wine production [3]. These wastes include marcs, pomace, and stems, which have a high residual concentration of polyphenols, compounds characterized by antioxidant and radical-scavenging properties [4]. In recent years, polyphenols have become interesting as reducing and stabilising agents in the reduction of metal ions into lower valence states under suitable conditions (e.g., temperature, concentration, pressure) [5]. Green synthesis, i.e., the chemical process exploiting natural compounds, is advantageous since it can reduce the production of organic waste or byproducts via the

development of environmentally friendly, dependable, and ecologically sustainable synthesis processes [6]. Plants, bacteria, fungi, algae, and other organisms are used in green synthesis [7]. Considering the different organic matrices, plant-derived wastes seem to be the most suitable choices, as they do not require any difficult or multi-step processes like isolation, culture preparation, or culture maintenance. In addition, synthesis occurs more quickly and cheaply in plants than in microbes.

Nanomaterials have gained significant attention for their unique physical and chemical properties, enabling applications in catalysis, magnetic materials, optical materials, biomedicine, and engineering [8]. Metal nanoparticles have recently been examined for their potential use as anti-wear and severe pressure additives in lubricating systems [9].

The addition of nanoparticles to lubricants, according to some studies, not only reduces the environmental impact of lubricants but also induces improvements in tribological qualities [10]. However, different factors, such as the size, shape, and concentration of the nanoparticles, affect how efficiently they reduce friction and prevent wear [11]. Indeed, the interaction between lubricants and surfaces is influenced by nanoparticles' chemical and physical characteristics [12]. Several metal oxides, such as  $\text{TiO}_2$ ,  $\text{CuO}$ ,  $\text{Fe}_3\text{O}_4$ ,  $\text{ZnO}$ , and  $\text{Al}_2\text{O}_3$ , have been used as lubricant additives [13]. Wu et al. [14] investigated the tribological properties of two lubricating oils with  $\text{CuO}$ ,  $\text{TiO}_2$ , and nano-diamond nanoparticles as additives. According to the results, adding  $\text{CuO}$  nanoparticles to standard oils improved their ability to reduce friction and prevent wear. Sphere-shaped nanoparticles may provide a rolling effect between the rubbing surfaces, converting the sliding friction to rolling friction. Heris et al. [15] (2020) observed that pure diesel oil with  $\text{ZnO}$  and  $\text{MoS}_2$  nanoparticles of different sizes showed superior anti-friction and anti-wear properties over pure lubricant. Bhaumik et al. [16] investigated the tribological properties of castor oil adding different  $\text{ZnO}$  concentrations between steel surfaces. A lower friction coefficient was observed for castor oil with respect to the commercial one, but no decrease was noticed with a concentration over 0.1 wt%. Battez et al. added  $\text{ZnO}$  to polyalphaolefin to study the influence on tribological behaviour. Under specific conditions,  $\text{ZnO}$  nanoparticles did not act as an anti-wear agent. By increasing pressure, they reduced wear after the first seizure load (localised melting of metal between two friction surfaces) [17]. Arumugam et al. evaluated how the two nano additives titanium dioxide ( $\text{TiO}_2$ ) and aluminium oxide ( $\text{Al}_2\text{O}_3$ ) improved the tribological characteristics of chemically treated rapeseed oil. It was found that chemically altered rapeseed oil with fibrous nano-alumina had a greater friction coefficient than that added with spherical nano-titanium dioxide [18].

In this paper, we describe an efficient and green method for preparing nano/micro  $\text{ZnO}$  particles. The effect of temperature, different Zn salts, and polyphenolic extracts obtained from pomace of two grape varieties, characterized by divergent polyphenolic profiles, on the structure of the obtained particles was evaluated by field emission scanning electron microscopy (FESEM), scanning electron microscopy (SEM), energy dispersive X-ray spectroscopy (EDX) and Fourier transform infrared (FTIR).

To examine their effect on friction and wear parameters in the presence of other common additives, the tribological potential of  $\text{ZnO}$  micro/nanoparticles was evaluated after the addition to a commercial lubricating oil used for lubricating piston gears.

The novelty of this study lies in the valorisation of two grape pomace extracts from winemaking by-products, differing in the amount of polyphenols and the study of their effect in the ecological synthesis of  $\text{ZnO}$  particles for tribological applications.

## 2. Materials and Methods

### 2.1. Materials

Pomace of two grape varieties was utilized for the preparation of the polyphenolic extracts: (i) Barbera, a red berry variety widely grown in the Piedmont Region (Cantina Tre Secoli, Mombaruzzo-AT, Italy) and (ii) Moscato, a yellow berry variety commonly used for the production of sparkling wine (Cantine Arione, Castiglione Tinella-CN, Italy).

Ethanol 95% was used for the extraction of polyphenols from grape pomace, methanol HPLC grade (VWR Chemicals, Radnor, PA, USA) and acetonitrile HPLC grade (Merck KGaA, Darmstadt, Germany) for the HPLC analysis of the extracts.

Zinc nitrate hexahydrate ( $\text{Zn}(\text{NO}_3)_2 \cdot 6\text{H}_2\text{O}$ ) 98% purity and zinc acetate dihydrate ( $\text{Zn}(\text{CH}_3\text{COO})_2 \cdot \text{H}_2\text{O}$ ) 98% purity (Acros organics—Thermo Fisher Scientific, Waltham, MA, USA) were used as starting material for the synthesis of the ZnO particles.

Natural-based oil Accu-Lube LB-500 (Accu-Lube®) was utilized for tribological tests.

## 2.2. Extract Preparation and Characterization

Grape pomace (GP) was subjected to pre-drying for 48 h at room temperature in a ventilated and dehumidified room, followed by drying at 40 °C in a ventilated oven for 48 h, up to constant weight (residual humidity 5–10%). Moscato seeds were manually separated from the GP and processed independently, while Barbera GP was processed as a whole (skins + seeds). The respective flours were obtained by grinding (1 min at ambient temperature). The extraction of polyphenols was performed with a hydroalcoholic solution (ethanol:water 1:1), according to a standardised green protocol [19] that allows for the complete recovery and reuse of the solvent which was itself a by-product of the wine industry. Briefly, 100 g of flour were extracted for 2 h with a 1:10 *w/v* ratio on an orbital shaker following sonication for 20 min (50 W, 48 kHz  $\pm$  10%). The suspension was then centrifuged for 20 min at 4000 rpm (2880 $\times$  *g*), at 18 °C, and the supernatant filtered twice with membrane filters of 5  $\mu\text{m}$  and 3  $\mu\text{m}$  mesh, respectively.

The filtered extracts were deprived of alcohol at 35 °C with a Genevac evaporator (EZ-2, Genevac©, Ipswich, UK) and then freeze-dried for 2 days at  $-50$  °C (Labconco FreeZone®, LABCONCO Corporation, Kansas City, MO, USA). All extractions were performed in duplicate.

Total polyphenols (expressed as gallic acid equivalents—GAE) and total anthocyanins (expressed as malvidin equivalents) were determined by UV-VIS spectrophotometry using the same methods described by Guaita et al. [19].

The total condensed tannins content, their mean degree of polymerization (mDP), and the percentage of each constitutive molecule were determined with the HPLC phloroglucinolysis method [20], following the operating protocol as reported by [21].

Monomer flavan-3-ols—(+)-catechin, (–)-epicatechin and (–)-epicatechin-3-O-gallate—and dimers B1 and B2 were determined by HPLC using a method for seeds analysis [22] modified as follows: The extract (2 mL) was acidified with  $\text{H}_3\text{PO}_4$  (40  $\mu\text{L}$ ), filtered with a 0.45  $\mu\text{m}$  polypropylene filter (VWR International, Milano, Italy) and injected (20  $\mu\text{L}$ ) in an ODS Hypersil RP-C18 reversed-phase HPLC column (200 mm  $\times$  2.1 mm I.D., 5  $\mu\text{m}$  packing, Thermo Scientific, Waltham, MA, USA), at 25 °C. The flow rate was 0.25 mL/min. Phase A was  $\text{H}_3\text{PO}_4$   $10^{-3}$  M and phase B was acetonitrile. The signal was monitored at 280 nm, and the peaks were identified by comparing the retention time and the UV absorption spectrum with pure standards. The concentrations of flavanols were determined using a six-point calibration curve obtained with pure standards.

To evaluate the method's repeatability and linearity, each standard was injected three times.

The content of hydroxy cinnamyl tartaric acids (HCTA) was determined according to [23]. Flavonols were determined using the same method but with signal monitored at 360 nm [24].

## 2.3. Synthesis of ZnO Particles

To synthesize ZnO particles, 0.07 g of each GP extract were dissolved into 160 mL of a hydroalcoholic solution (EtOH:H<sub>2</sub>O 1:1) and stirred for 2 h at room temperature. Then 2.9 g of zinc nitrate hexahydrate ( $\text{Zn}(\text{NO}_3)_2 \cdot 6\text{H}_2\text{O}$ ) and 2.14 g of zinc acetate dihydrate [ $\text{Zn}(\text{CH}_3\text{COO})_2 \cdot 2\text{H}_2\text{O}$ ] were added to the solution.

The suspensions were then dried at 150 °C until they were reduced to a paste and heated in a muffle furnace at 500 °C or 600 °C for two hours. Figure 1 shows the overall

procedure for the preparation of the ZnO particles, while a list of the prepared samples is presented in Table 1.

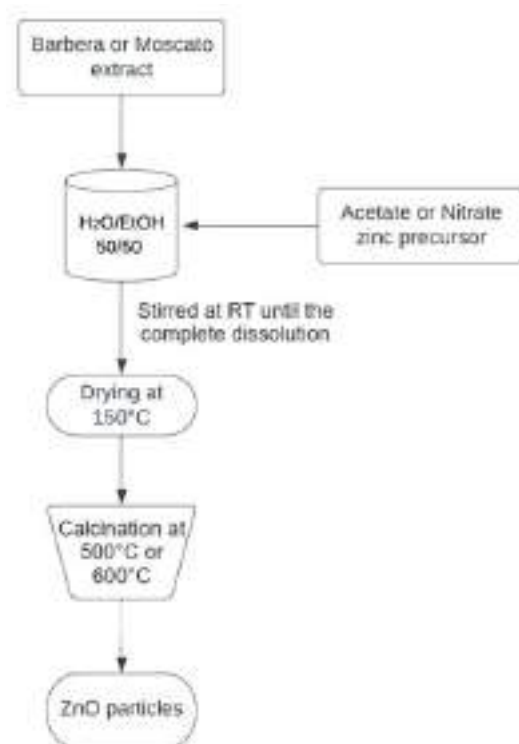


**Figure 1.** Flowchart illustrating the procedure for the preparation of ZnO particles using polyphenolic extracts from grape pomace.

**Table 1.** Summary of the different preparation methods used in the synthesis of ZnO particles. For all the synthesis a EtOH:H<sub>2</sub>O 1:1 *v:v* solution was utilized and a temperature of 150 °C were utilized for the drying step.

Sample Name	Extract	Zinc Salt Precursor	Calcination Temperature
BA500	Barbera	Zinc acetate	500 °C
BA600	Barbera	Zinc acetate	600 °C
BN500	Barbera	Zinc nitrate	500 °C
BN600	Barbera	Zinc nitrate	600 °C
MA500	Moscato	Zinc acetate	500 °C
MA600	Moscato	Zinc acetate	600 °C
MN500	Moscato	Zinc nitrate	500 °C
MN600	Moscato	Zinc nitrate	600 °C

#### 2.4. Characterization of ZnO Particles

Powder X-ray Diffraction (XRD) was used to examine the crystalline structure of the ZnO particles. XRD patterns were recorded on an X-ray diffractometer Malvern Panalytical X'Pert Pro (Malvern, UK) equipped with an X'Celerator detector powder diffractometer using Cu K $\alpha$  radiation ( $\lambda = 0.154$  nm) generated at 45 kV and 40 mA within a  $2\theta$  range of 20–80°. The patterns were compared to standards compiled by the Joint Committee on Powder Diffraction and Standards (JCPDS), Card No. 36-1451. The average size of diffracting domains and the microstrain ratio were then determined by Rietveld refinement using the MAUD program. The size, shape, and elemental composition of the particles were evaluated by field emission scanning electron microscopy (FESEM TESCAN S9000G (Brno, Czech Republic) and a ZEISS EVO 50 XVP with LaB<sub>6</sub> source) both equipped with Energy Dispersion Spectroscopy (EDS) probe for elemental analysis. Before the analysis,

samples were coated with a 5 nm thick Au layer. FTIR spectra of the extracts and the obtained ZnO particles were recorded by JASCO spectrophotometer using a KBr pellet in the range of 4000–400  $\text{cm}^{-1}$  with a spectra resolution of 4  $\text{cm}^{-1}$ .

### 2.5. Wear Test

To investigate the effect of ZnO particles added to a lubricant on the friction coefficient and wear, tribological tests were conducted using an HT tribometer (CSM Instruments, Switzerland). Ball-on-disc tests were carried out using an alumina ball against an X45CrSi9-3 stainless steel disc (Table 2), mainly used as valve material in the automotive industry. Tests were conducted for a total distance of 20,000 laps (754 m) at a constant sliding speed of 20 cm/s under 10 N applied load.

**Table 2.** Nominal composition in wt% of X45CrSi9-3.

Fe	C	Si	Mn	Cr	Ni	P	S	W	Co
Bal.	0.4–0.5	2.7–3.3	≤0.8	8–10	≤0.6	≤0.22	≤0.03	-	-

These conditions were chosen based on tribological data present in the literature for similar systems, in order to have a measurable wear amount [25]. For this purpose, a vegetable-based oil (Accu-Lube™ LB 5000 with a density of 8.5 g/mL and a viscosity of 18  $\text{mm}^2/\text{s}$ ) was used, without additional additives. Particle-fluid mixtures were prepared using 0.5 wt% ZnO particles dispersed in the vegetable-based lubricant using a magnetic stirrer plate, working at RT. The trace depth and volume of material removed after the tribological test were assessed with a contact profilometer (Form Talysurf 120- Taylor Hobson, UK), equipped with a 2  $\mu\text{m}$  diamond conical stylus. Specific wear rates ( $k$ ) were obtained by normalising the estimated wear volume to the load.

$$k = V / SL \quad (1)$$

where the volume loss ( $V$ ) is expressed in  $\text{mm}^3$ ,  $S$  is the total sliding distance in meters and  $L$  is the applied load in Newtons. Each test was carried out three times.

## 3. Results and Discussion

### 3.1. Characterization of Moscato Seeds and Barbera GP Extract

The polyphenolic composition of Barbera GP and Moscato seeds extracts differed both qualitatively and quantitatively (Table 3).

The Moscato extracts resulted significantly richer in polyphenolic compounds than Barbera one (Table 3), mainly due to the differences in winemaking technique: generally, white grape pomace is not fermented; therefore, it maintains the original polyphenolic composition of fresh grapes; conversely, red grape pomace is fermented and macerated during winemaking; therefore, its polyphenolic content is reduced compared to fresh grapes. On the other hand, Barbera extracts contained anthocyanins, HCTA, and flavonols, that were absent in Moscato seeds extracts. These differences are due to the different natural distribution of these molecules in the berry [26]. Qualitative differences in the composition of condensed tannins were also observed: Barbera tannins had lower mDP (mean degree of polymerization), a lower percentage of gallates subunits, and different proportion between (+)-catechin and (−)-epicatechin compared to tannins of the Moscato seed extract.

The extract of Barbera GP showed similar FTIR absorption band to those of the Moscato seeds, though with some slight differences (Figure 2). In particular, in the range 3500–3250  $\text{cm}^{-1}$ , a similar U-shaped band can be observed for both extracts, attributable to the OH stretching of alcohols and phenols. The region between 2945 and 2845  $\text{cm}^{-1}$  showed a difference between the two extracts for the signals related to the stretching of symmetric and asymmetric C-H bonds of  $\text{CH}_2$  and  $\text{CH}_3$  groups.

**Table 3.** Content of major polyphenolic compounds determined in the extract of Barbera GP and Moscato seeds. All parameters are expressed as mg/g dry weight of freeze-dried extract, except for mDP (mean degree of polymerisation) and the percentage subunit composition of condensed tannins. HCTA and flavonols are reported as the respective sum of the single molecules (as mg/g dry weight of freeze-dried extract).

Polyphenolic Category	Polyphenolic Profile	Barbera	Moscato
	Total polyphenols (GAE)	219.6 ± 4.98	540.0 ± 2.71
	Total anthocyanins	25.9 ± 2.05	-
Condensed tannins (polymeric flavan-3-ols)	Condensed tannins	63.2 ± 4.21	340.1 ± 8.86
	mDP	3.8 ± 0.05	4.4 ± 0.06
	gallates %	14.9 ± 0.26	20.1 ± 0.06
	(+)-catechin %	32.4 ± 0.42	20.4 ± 0.03
	(-)-epicatechin %	67.6 ± 0.42	79.6 ± 0.03
monomeric flavan-3-ols	(+)-catechin	1.8 ± 0.05	15.6 ± 0.03
	(-)-epicatechin	1.4 ± 0.05	10.4 ± 0.27
dimeric flavan-3-ols	dimer B1	0.4 ± 0.02	2.5 ± 0
	dimer B2	1.4 ± 0.01	2.0 ± 0.13
	gallic acid	2.3 ± 0.04	3.1 ± 0.01
	∑HCTA	2.6 ± 0.04	-
	∑flavonols	5.4 ± 0.05	-

The signals detected in the range between 1611 and 1441  $\text{cm}^{-1}$  were assigned to the stretching of the aromatic ring, whereas the weak band observed between 1400 and 1000  $\text{cm}^{-1}$  can be ascribed to the overlapping of the signals relating to the bending of the C-H and O-H bonds. Peaks related to the bending of the aromatic ring were observed in the region between 850 and 500  $\text{cm}^{-1}$ . The major difference between the two extracts can be observed in the region relating to the stretching of the carbonyl bonds. In fact, for the Barbera GP extract, it was possible to observe a peak at 1717  $\text{cm}^{-1}$  relating to the stretching of carboxyl C=O, while for the Moscato seed extract, a sharp peak occurred at 1745  $\text{cm}^{-1}$  attributable to the presence of ester C=O stretching, related to the presence of fatty acids and their glycerides. Indeed, compared to grape skins, the content of the seeds is highly lipophilic and fatty acids are mainly present as glycerides [27].

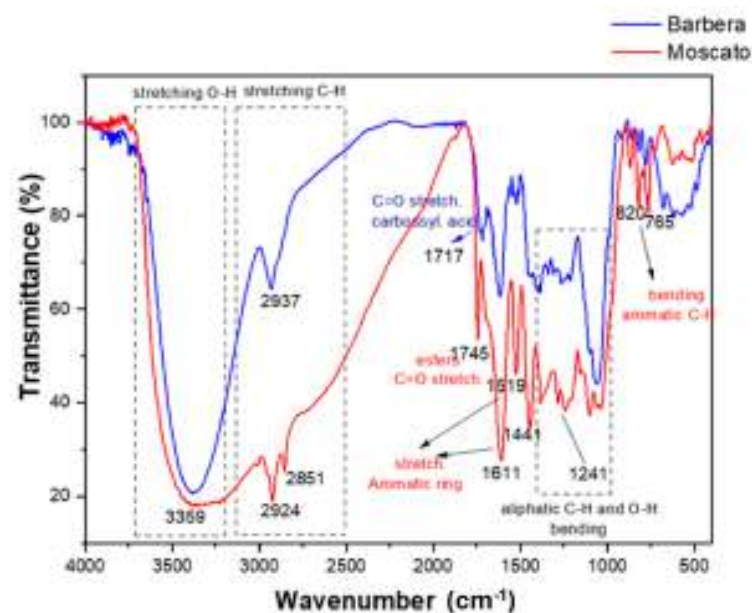


**Figure 2.** FTIR spectra of Barbera GP and Moscato seeds extracts.

### 3.2. FTIR Analysis of ZnO Nanoparticles

FTIR spectra obtained for all kinds of ZnO particles were characterized by the formation of a band in the range 580–420  $\text{cm}^{-1}$  (Figure 3). The band is characteristic of the bulk vibrations of the O-Zn-O bond, which confirms the identity of the particles obtained for both nitrate and acetate zinc precursors. No significant differences between the ZnO particles were observed. Weak peaks related to the vibrations of  $\text{CH}_2$ , C-C, C-OH, and C=C can be observed at 2920, 2850, 1640, 1480, and 1387  $\text{cm}^{-1}$  and could be related to carbonaceous material adsorbed on the particle's surface. In addition, further peaks attributable to the surface adsorption of moisture (peak at 3450  $\text{cm}^{-1}$ ) and to  $\text{CO}_2$  present in the atmosphere (peak at 2340  $\text{cm}^{-1}$ ) were observed but did not provide useful information on the materials.

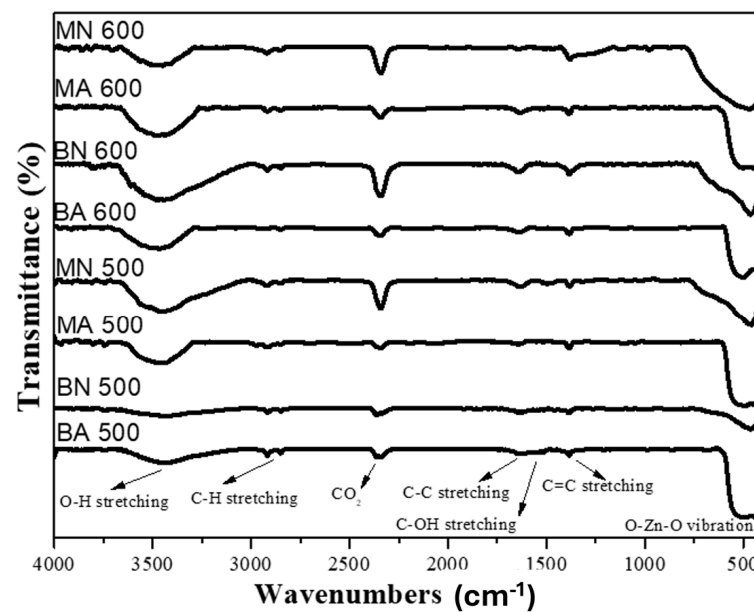


**Figure 3.** FTIR spectra of ZnO particles prepared from zinc acetate or zinc nitrate using Barbera GP or Moscato seeds extracts as catalyst.

### 3.3. X-ray Diffraction Analysis of ZnO Particles

Peak positions in the XRD pattern of the ZnO particles closely matched those of the hexagonal wurtzite polycrystalline ZnO phase (ICSD database no. 36-1451, Sp. Gr. P63mc, hexagonal,  $a = 3.2498$  and  $c = 5.2066$ ) (Figure 4). The absence of any other peak demonstrated that no crystalline impurities were present in amounts higher than 1% (the sensitivity level of the XRD technique) [28]. The diffraction peaks were sharp and narrow, indicating that the metal oxide was crystalline [29]. The diffraction peaks were evident, with the exception of peak 004, which in the BA600 sample was almost negligible. Very small differences were observed in the relative intensity of the peaks among the different samples. To evidence any preferred orientations, the intensity ratios (100/002) are shown in Table 4.

**Table 4.** Intensity Ratio 100/002 of XRD peaks.

Standard ZnO (JCPDF: 36-1451)	BA 500	BA 600	BN 500	BN 600	MA 500	MA 600	MN 500	MN 600
1.29	1.29	1.09	1.06	1.04	1.02	1.02	1.02	1.01

Comparing the 100/002 intensity ratio of the peaks, which allows showing any preferred orientation of the crystal, it emerged that, except for BA500, ZnO synthesised with both extracts led to a lower ratio compared to the standard oxide, indicating preferential

growth along the c-axis [30]. Moreover, the ratio for ZnO obtained with Moscato seeds was also lower than that of particles synthesised with Barbera GP. As reported in the literature, the strong (0 0 2) peak, represented by the small (100)/(002) ratio, indicates crystal growth along the c-axis, whereas the big (100)/(002) ratio indicates shortening growth along the c-axis. Fitting the diffractogram data by Rietveld using an isotropic model for the ZnO samples confirmed that all synthesized ZnO had a hexagonal structure with space group P63mc (Figure 5). The solid black line is the MAUD fit, the dots represent the experimental data, while the solid line beneath the diffractogram corresponds to the difference between the calculated and observed intensities. The weighted profile R-factor, profile R factor, and goodness of fit  $\chi^2$  parameters, utilized to determine the fit between the theoretical and experimental diffractograms, are reported in Table 5 together with the lattice and structural parameters: crystallite size (D) and microstrain ( $\epsilon$ ).

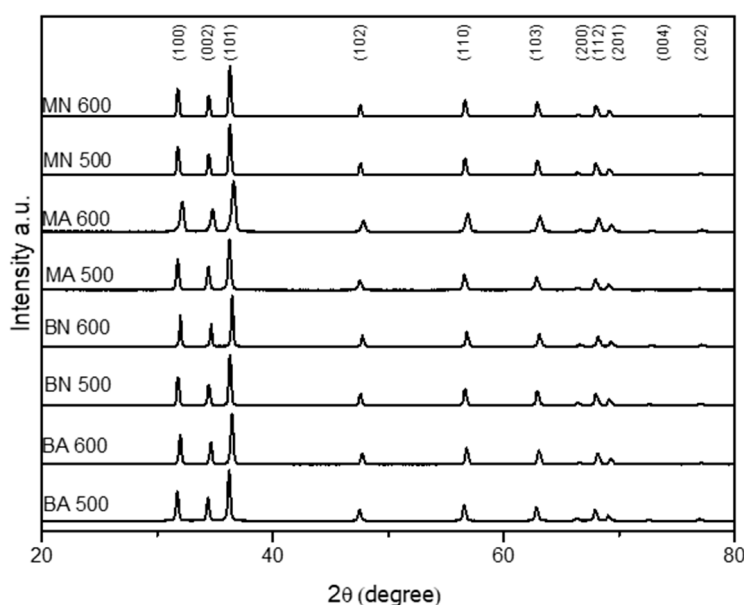


**Figure 4.** XRD pattern of ZnO particles obtained from Barbera GP (B) or Moscato seeds (M) extracts and utilising acetate (BA or MA) or nitrate (BN or MN) as precursors and synthesized at 500 and 600 °C.

**Table 5.** Reliability parameters of the fit (Rwp, Rp and  $\chi^2$ ), lattice and structural parameters of ZnO obtained from Rietveld refinement.

	D (nm)	$\epsilon$	a (Å)	c (Å)	Rwp (%)	Rp (%)	$\chi^2$
BA 500	65.61	$2.876 \times 10^{-4}$	3.251	5.208	12.526	6.77	1.834
BA 600	70.76	$2.180 \times 10^{-4}$	3.252	5.209	9.548	7.33	1.915
BN 500	96.7	$2.030 \times 10^{-4}$	3.249	5.206	8.819	6.57	1.921
BN 600	155.62	$7.387 \times 10^{-4}$	3.252	5.210	9.993	5.95	1.962
MA 500	54.18	$2.189 \times 10^{-4}$	3.250	5.208	8.417	5.98	1.625
MA 600	58.24	$3.289 \times 10^{-4}$	3.256	5.218	12.701	10.03	1.781
MN 500	90.4	$2.006 \times 10^{-4}$	3.250	5.207	11.577	8.87	1.985
MN 600	105.59	$1.964 \times 10^{-4}$	3.249	5.206	13.031	6.98	1.718

Rwp: Weighted residual error; Rp: profile factor;  $\chi^2$ : goodness of fit.

The a and c refined values of the lattice parameters of ZnO particles were very close to those of the standard (a: 3.249; c: 5.206) except for MA600 which showed higher values for both parameters. An increase in the number of defects, including vacancies and dislocations, inside nanoscale crystallites, might be connected to a rise in lattice parameters [31]. Crystallite sizes were very different among the ZnO samples (Table 5).



Interestingly, crystallite size increased as the synthesis temperature raised when nitrate was used as precursor, while only slight differences were observed in the case of acetate [32,33]. This is evident in particular for BN500, increasing from 96.7 nm to 155.62 nm. Moreover, the ZnO synthesized using nitrate as a precursor showed a higher crystallite size with respect to those synthesized using acetate, as already reported in the literature [34]. The influence of precursor, temperature, and extract type on the microstrain is unclear. However, all samples except BN600 showed a comparable microstrain value, ranging between 1.96 and 2.18.

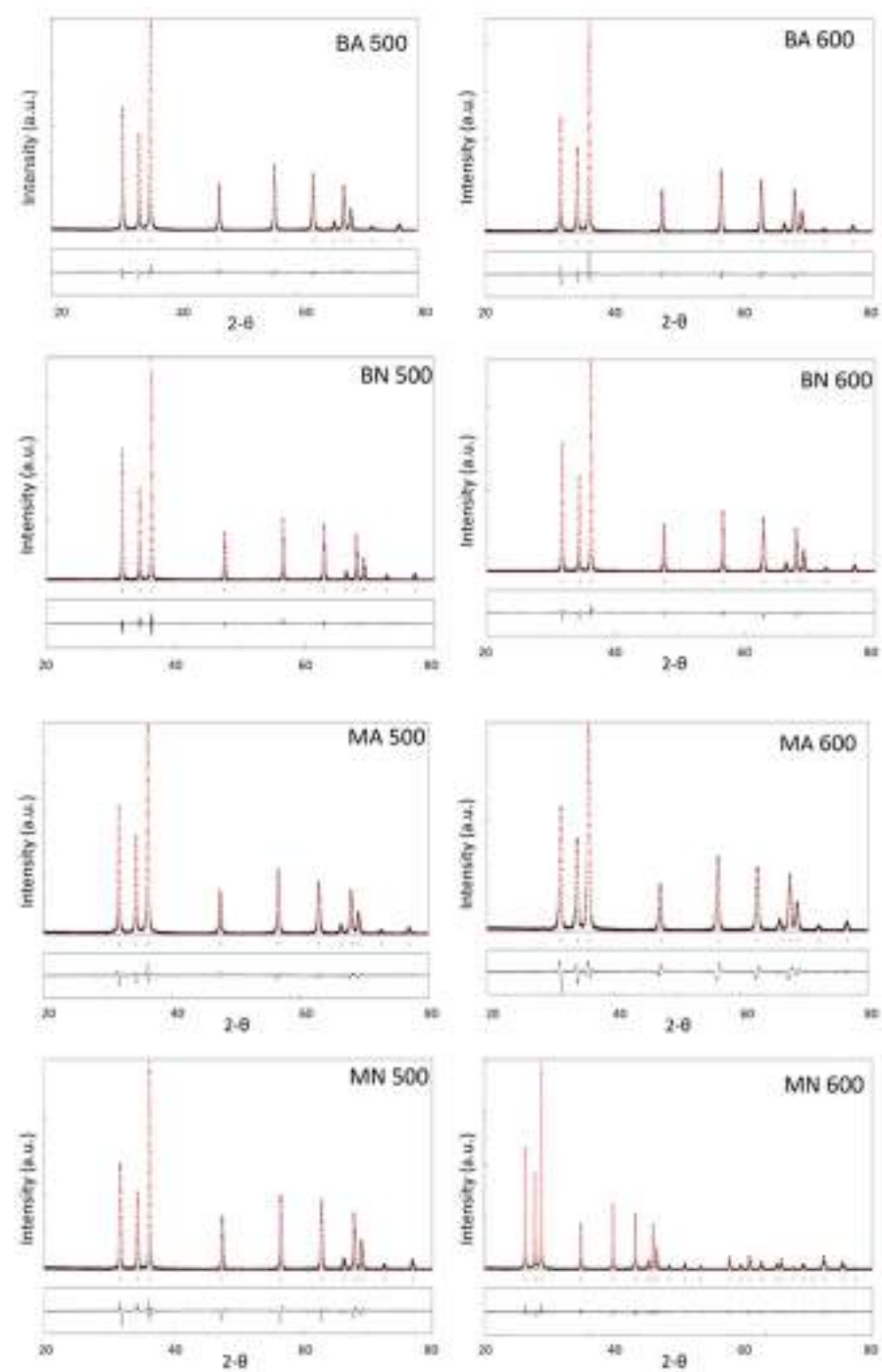


**Figure 5.** XRD diffractogram with Rietveld refinement of the ZnO particles. The dots represent the experimental data, calculated (full line) while the solid line beneath the diffractogram corresponds to the difference between the calculated and observed intensities.

### 3.4. Morphological Analysis

The precursors used in the synthesis affected the size and shape of the particles (Figures 6 and 7). Indeed, quite regular-shaped nanoparticles with a size between 50 and 200 nm were formed when zinc acetate was used in the reaction (Figure 6a–d), while pyramid-like particles of 10 to 20 microns were obtained with zinc nitrate (Figure 7a–d).

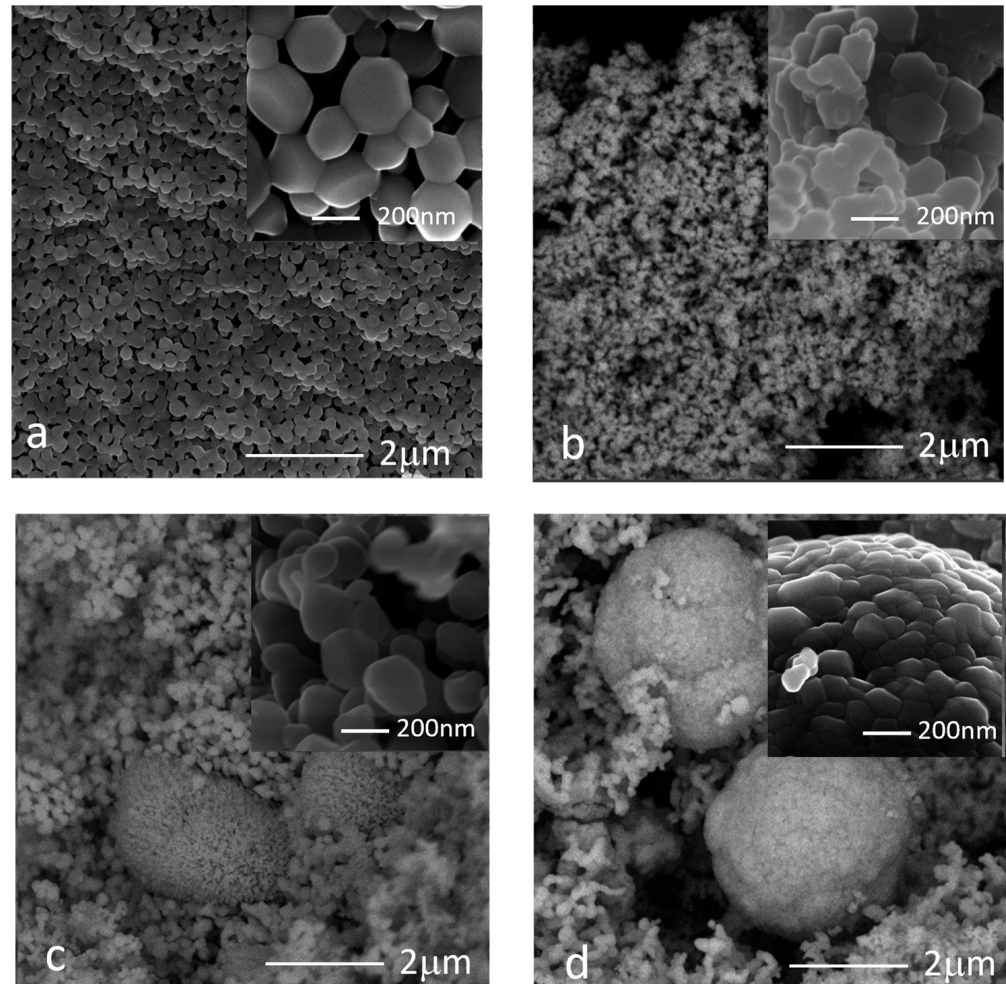


**Figure 6.** FESEM micrographs of ZnO synthesized using Zn acetate as a precursor: (a) BA500, (b) MA500, (c) BA600 and (d) MA600. (B: Barbera; M: Moscato).

Barbera GP extract favoured a higher homogeneity in shape and size than Moscato seed extract (Figure 6), which induced the formation of both round/spherical and hexagonal nanoparticles. ZnO synthesized using acetate at 600 °C with Moscato seed extract were densely packed, almost as if they were sintered.

Considering particles obtained using zinc nitrate (Figure 7a–d), a preferably bipyramidal shape was obtained. However, when the Moscato seeds extract was used, the co-presence of spherical nanoparticles with dimensions of about 20–30 nm was observed (MN500 and MN600, Figure 7b,d). The different shape and size of the particles obtained with the two polyphenolic extracts could be related to their composition. The Moscato seeds extract was characterized by a higher concentration of total polyphenols than Barbera GP extract and as evidenced by FTIR analyses, it contained fatty acids in the form of triglycerides which could be responsible for the observed different morphologies of the ZnO particles [35].

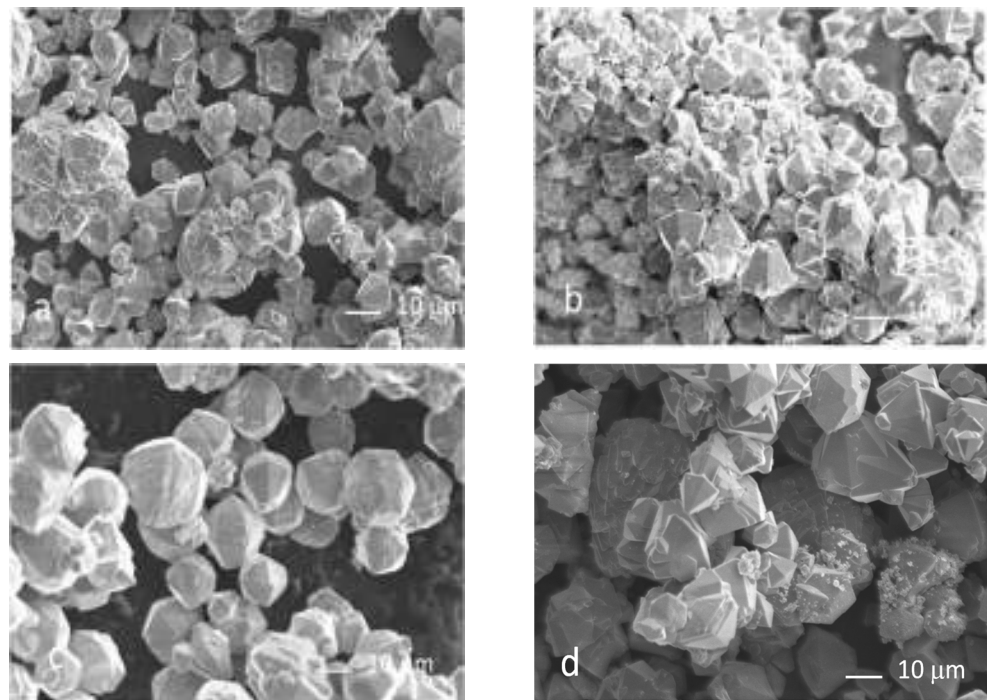


**Figure 7.** SEM micrographs of ZnO synthesized using Zn nitrate as a precursor: (a) BN500, (b) MN500, (c) BN600 and (d) MN600. (B: Barbera; M: Moscato).

The literature reports several examples of the synthesis of ZnO nanoparticles starting from Zn nitrate and/or acetate assisted by the presence of natural extracts rich in polyphenols [36,37]. In these works, it is often reported that rounded shaped particles are obtained, whose dimensions are in the order of 50–100 nm. Among these, the work of Bandeira et al. [38] reports, as in our case, a different morphology and size between the ZnO particles obtained from the two different precursors. In their case, the *Ilex Paraguensis* extract led to the formation of spherical nanoparticles when the precursor was zinc nitrate, while the use of zinc acetate led to particles of micrometric dimensions and with an irregular morphology. In our case, both the Barbera and Moscato extracts led to the formation of spherical particles when the precursor was zinc acetate (BA and MA), while the use of zinc nitrate produced micrometric particles whose morphology is similar to a bipyramidal shape (BN and MN). This observation would suggest that the interaction between the extract matrix and the precursor (probably the counterion) is crucial in the formation of the particle. A better interaction between the extract matrix and the precursor leads to the formation of smaller rounded-shaped particles. On the contrary, when the interaction between precursor and extract is not optimal, bigger particles with an irregular morphology are formed.

### 3.5. Tribological Tests

The evolution of the friction coefficient (COF) as a function of the sliding distance (m) of the lubricant oil with ZnO particles is shown in Figure 8. In both graphs, the coefficient of friction of the oil without the addition of ZnO is shown as reference (curve named “base oil”). The graphs are split by type of precursor, acetate (a) and nitrate (b), to make the evolution of the coefficient of friction clearer. The results of the average coefficient of friction and the standard deviation, representing the test fluctuation, are presented in Figure 9. The addition of ZnO particles within the lubricant oil led to a stabilization of the friction coefficient (COF) and to a shorter running-in period (almost absent) when using particles obtained with both Zn acetate (Figure 8a) and Zn nitrate (Figure 8b) in comparison to the reference base oil.

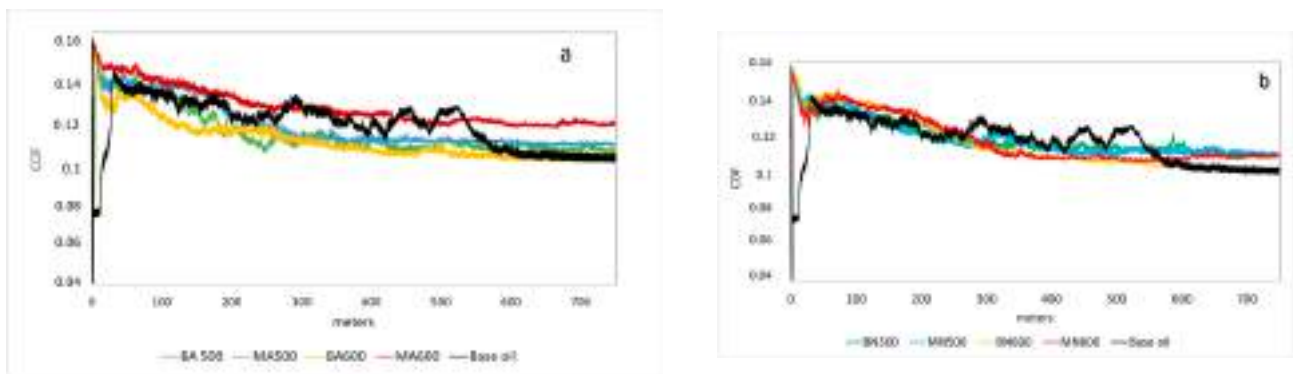


Figure 8. Friction evolution of ZnO synthesized using (a) acetate and (b) nitrate.

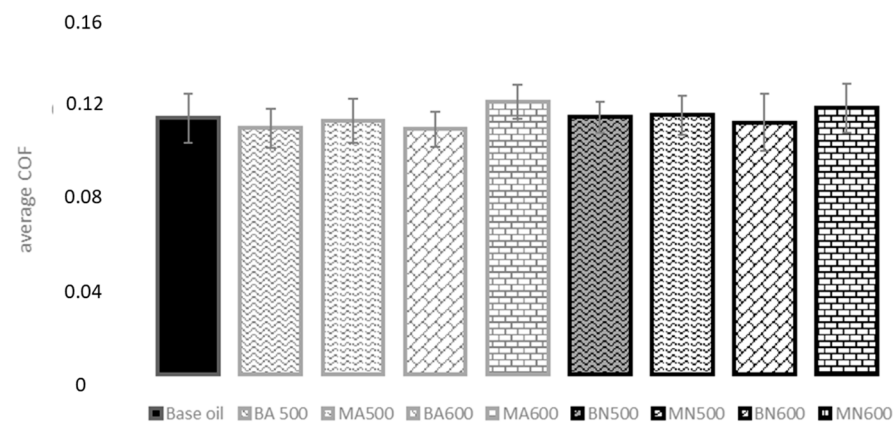


Figure 9. Average friction coefficient of base oil and base oil mixed with synthesized ZnO.

The most relevant difference concerned the friction behaviour when MA600 was added to the oil. Indeed, the COF was higher than that of the base oil during most of the sliding test.

This behaviour can be explained by considering that ZnO nanoparticles, synthesized using Moscato and acetate at 600 °C (MA600), tend to form large aggregates that can hardly fill the valleys between the asperities of the sliding steel pair, thus producing a relatively high coefficient of friction.

This should result in increased drag in the contact zone. Increased entrapment resistance would result in a build-up of debris at the entrance of the valley and a lack of lubricant within the contact [39].

The differences were less pronounced among other samples produced using acetate (Figure 8a). BA600 showed the lowest COF, overlapping with the base oil at the end of the test, while BA500 and MA500 showed very similar behaviour, approaching the base oil COF at the end of the test. The COF with particles obtained with Moscato seed extract was slightly higher with respect to particles synthesized using acetate and Barbera GP.

The COF obtained by adding BN600 and MN600 to the oil (Figure 8b) showed a similar trend up to a distance of 400 m, diverging in the last part of the test. BN500 and MN500 had a very similar trend, although the latter was more unstable.

Nevertheless, comparing the two polyphenolic extracts, the COF obtained by adding ZnO synthesized using Barbera GP extract showed a slightly lower friction coefficient than the particles synthesized using Moscato seed extract.

Concerning friction coefficient results, the behaviour appears dependent on particle size and agglomeration degree, resulting in a theoretically thicker fluid film. For the particles obtained with acetate, their small size allowed them to fill the valleys of the

interacting surfaces. In addition, nanoparticles tend to develop a three-body rolling mechanism between interacting surfaces. Both effects can positively affect the friction coefficient, stabilizing it with respect to base oil [13]. Also for microparticles, the rolling effect between the interacting surfaces can explain the friction coefficient stabilization.

Figure 10 shows a comparison of the wear results of the base oil and the same oil containing the synthesised ZnO particles. It can be seen that oil containing MA600 and MN600 particles showed lower wear resistance than the standard, while the other samples induced higher resistance. Particles (MN600) and nanoparticles (MA600) in the form of aggregates produced a deformed layer to varying degrees within the wear scar. The aggregates were occasionally removed from the wear scar in the form of broken or delaminated ‘debris’ leading to high wear.

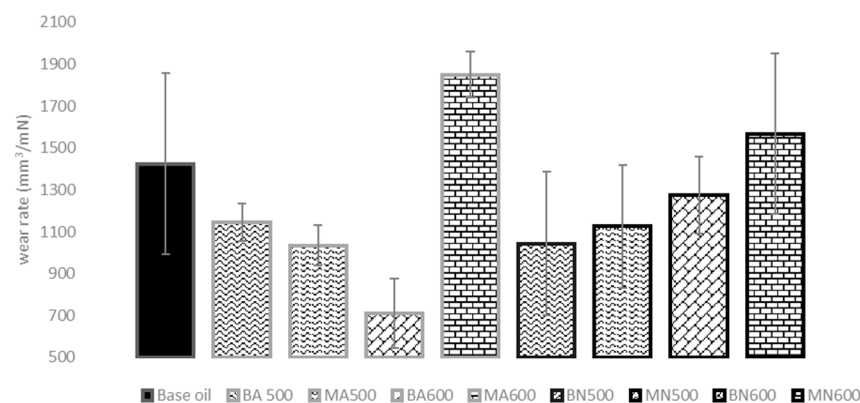


**Figure 10.** Wear rate of base oil and base oil mixed with synthesized ZnO.

A certain impact of the synthesis temperature can be observed: a higher mean wear rate occurred for particles obtained with both extracts at 600 °C compared to those synthesized at 500 °C when the nitrate salt was used. In the case of the acetate salt, this effect was observed only with the ZnO synthesized with Moscato seeds extract, while the opposite resulted when using Barbera GP extract. Similarly to friction behaviour, the differences in wear and friction behaviour can also be related to both the different morphology and the tendency to aggregate of the particles depending on the diverse sintering temperatures.

In fact, the rolling and exfoliation processes of the particles are restricted by the aggregation/agglomeration phenomena, which have an adverse effect on their efficacy and their capacity to lessen wear and stabilize friction. The consequence of the different morphologies and tendency to agglomeration was seen not only on friction but also on surface damage between contacting components. SEM analyses of the surface of the wear track, reported in the following section, indicated the presence of grooves, scars, and debris on the surface of the contact track.

Spherical nanoparticles act most effectively as ball bearings between friction surfaces, but in the case of particles with various sizes and shapes, different contacts between the sliding surfaces are produced, thus changing the tribological behaviour.

It can be concluded that the extract origin, i.e., its composition, could also have a possible impact on these characteristics. Indeed, particles obtained with Zn acetate and Barbera GP, irrespective of the temperature of synthesis, exhibited reduced wear and a lower coefficient of friction likely due to their tiny and relatively uniform size. Instead, the particles obtained with the Moscato seeds extract resulted in inducing a lower wear than that of standard oil when the synthesis occurred at 500 °C, but the friction stabilization was delayed. The same extract, but with the synthesis at 600 °C, provoked aggregation of the particles, resulting in high wear and friction. The effect of the synthesis temperature on particle aggregation, and thus friction and wear, was also observed when nitrate was used as a precursor (i.e., MN600 sample), thus confirming the impact of the interaction between the synthesis parameters and the extract composition on the tribological characteristics.

Such effect shall be taken into consideration when developing and assessing polyphenolic extracts from other sources. Indeed, it is known that particle aggregation can produce new asperities, increasing friction and wear, leading to the formation of crack points (micro-pits and macro-spalls) [40], which, subjected to the stress along the test, would grow in number and size provoking the removal of a greater amount of material from the wear surface.

The same debris generated by these processes can further act as abrasive material. Confirmation of the particle morphology effect could be observed by comparing COF and wear from MN500 and BN500.

The inhomogeneity of the MN500 particles, due to the presence of both micrometric and nanometric particles, may have induced the observed negative effect, as the different sizes cause different abrasive conditions.

On the other hand, the presence of nanoparticles, as in the case of those obtained from Barbera GP and acetate salt, could induce a repairing effect as observed in other studies [40], though depending on shape and size, since they can fill cracks that form on the material surface and thus delay the formation of further surface defects, increasing the resilience of the material toward wear.

### 3.6. Worn Morphology

Wear surfaces are shown in Figure 11. Since the differences among EDS spectra were limited, only the spectra of the steel with base oil and the oil plus MA600 are shown, being the most relevant. The most evident phenomena for all samples, albeit to different degrees, was the plastic deformation due to the coupling between the alumina ball and the steel disc, whose different hardness led to the formation of grooves on the softer material.

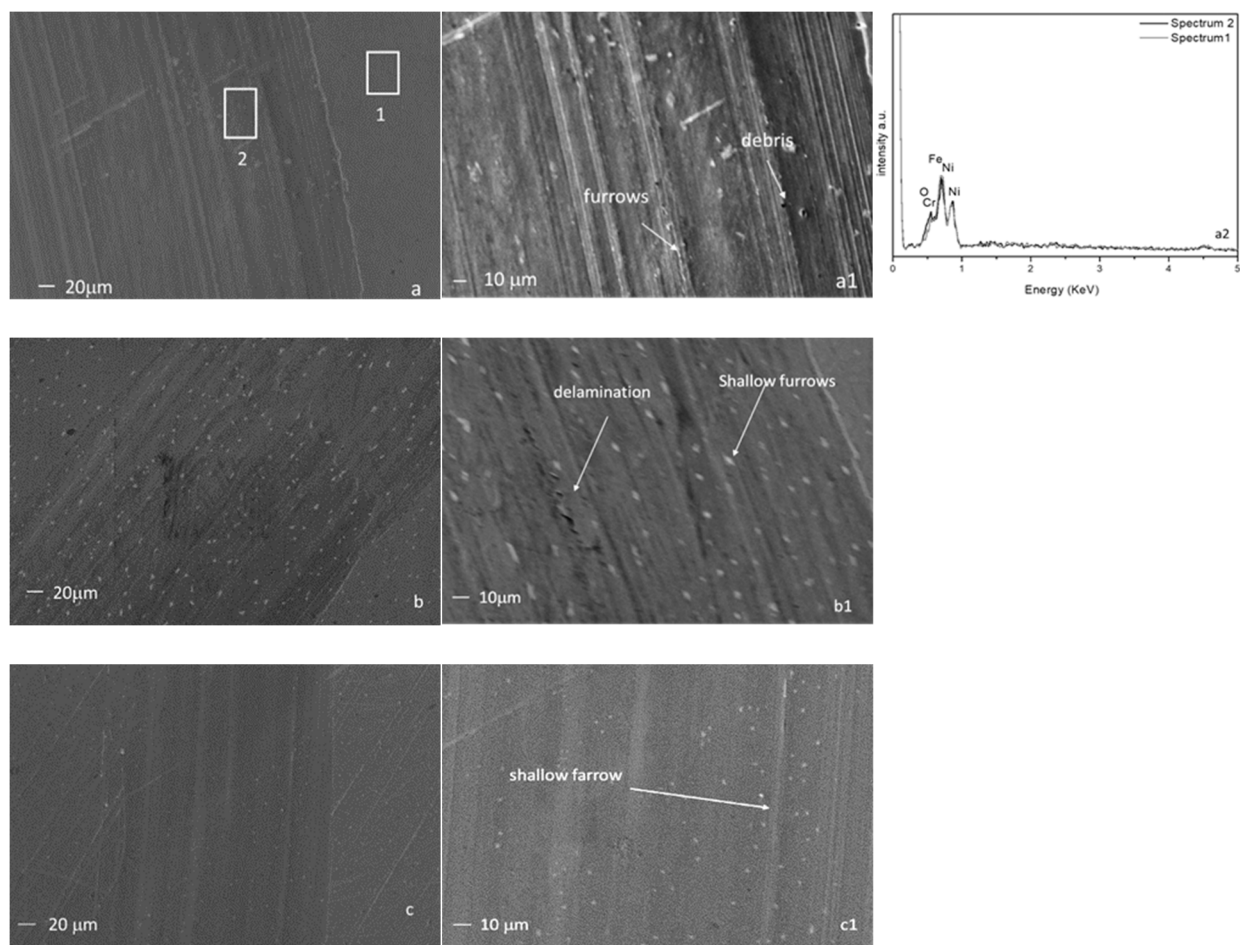


Figure 11. Cont.

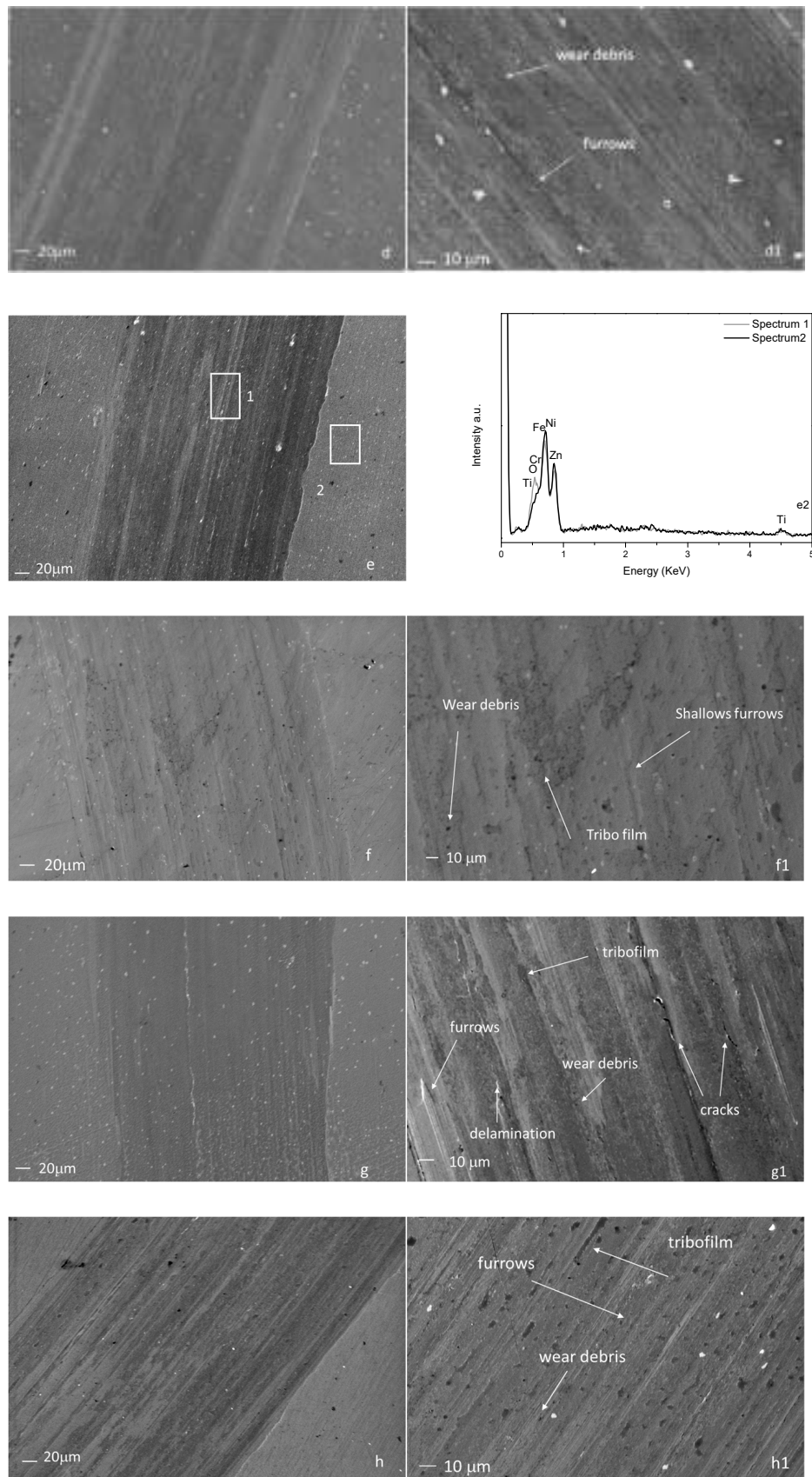
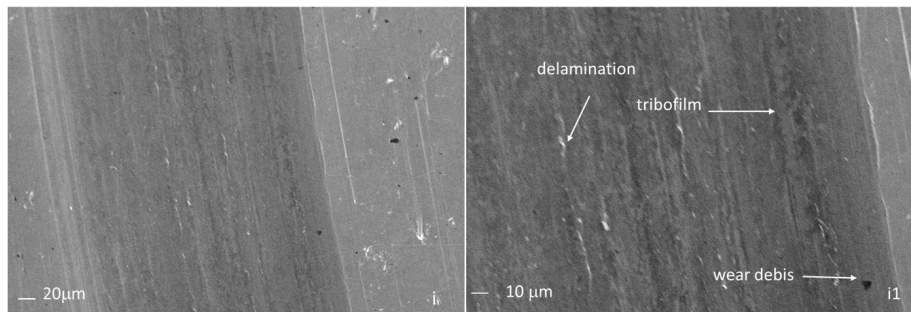


Figure 11. Cont.



**Figure 11.** (a) base oil, (b) BA500, (c) BA600, (d) MA500, (e) MA600, (f) BN500, (g) BN600, (h) MN500, (i) MN600.

The surface morphology of the steel lubricated with pure base oil (Figure 11a) revealed a significant region with numerous deep furrows parallel to the sliding direction and a lot of wear debris. These grooves likely formed as a result of worn debris being trapped when the asperities broke or were ploughed during sliding. All these phenomena on the worn disc surface support the results of the high friction coefficient and wear rate, as shown in Figures 8–10. Comparing the EDS spectra (Figure 11(a2)), a slight increase in oxygen was observed inside the wear track with respect to the external area, indicating oxidation phenomena during the wear test.

With regard to BA500 (Figure 11(b,b1)), some delamination and small grooves were observed, but, generally, the surface appeared smoother than with the base oil. The width of the wear groove decreased significantly, and the ploughing effect was significantly less noticeable for oil containing BA600, as shown in Figure 11c, explaining the overall improvement in friction stabilization and anti-wear characteristics of the oil, according to the tribological data discussed in the previous section. In both samples, ZnO particles adhered to the surfaces, supporting the hypothesis that nanoparticle addition to oil can induce a repairing effect by filling cracks [41] and hindering the formation of further cracks. Figure 12 shows a SEM image and corresponding EDS spectrum of sample BA600 where the presence of ZnO on the surface is highlighted. Furrows and wear debris can be observed within the track also for MA500 (Figure 11d), but in this case, no delamination phenomena were present, unlike with BA500.

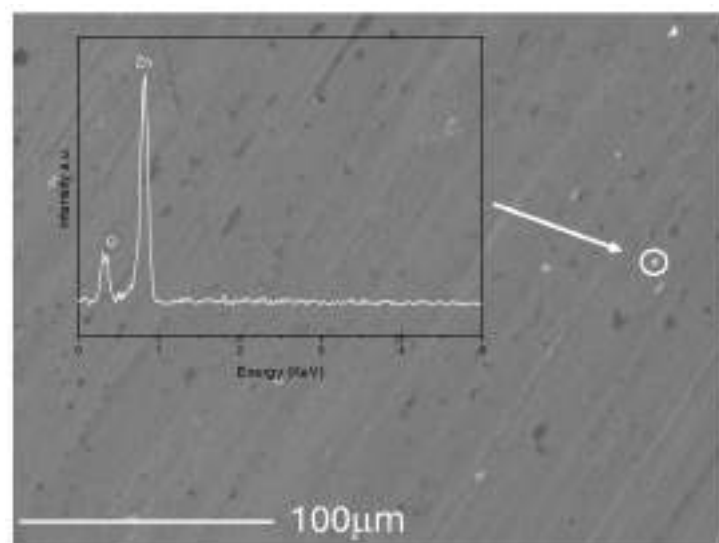


**Figure 12.** Detail, with EDS, of MN500 wear track. White circle highlights the white particle where the EDS spectrum was acquired.



An explanation for the nanoparticles' anti-wear mechanism may be found in the scenario where the oil layer between the worn surfaces decreases during the mixed lubrication regime. In such cases, the worn surfaces can be separated by the nanoparticles, which can act as load bearing, then avoiding adhesion [42].

The steel surface obtained after using MA600 resulted in the most worn (Figure 11(e,e1)), full of wear debris and showing many deep furrows, microploughs, and delamination, which suggest the presence of plastic deformation [43]. The friction and wear coefficient increased in this case likely due to the agglomeration of the nanoparticles probably caused by the high synthesis temperature (600 °C). As a consequence, the agglomeration of the particles led to an unstable oil supply between the sliding pairs, and thus a transition could occur from a mixed lubrication regime to a boundary regime and vice versa [16]. Furthermore, small amounts of tribofilm can be observed (Figure 11(e1)). It could be hypothesized that ZnO particles of higher size abraded the steel surface, leading to the formation of the small amount of tribolayer.

Similarly to bare oil, EDS (Figure 11(e2)) showed no substantial difference between outside and inside of the track except for an increase in the oxygen peak, thus indicating oxidation occurrence as a consequence of the sliding test.

With regard to microparticles, i.e., those obtained from nitrate salt, a similar mechanism was observed by adding ZnO to oil, but in this case, being bigger than ZnO deriving from acetate, they did not act as a filler but merely supported the pressure of the ball. In addition, the bigger ZnO particles resulted in more pronounced abrasion of the steel surface, inducing the formation of a higher amount of tribofilm. This phenomenon was observed adding BN500 (Figure 11(f,f1)) to the oil, resulting in a surface covered with wear debris and shallow furrows. Moreover, the surface was covered by a tribofilm of different entities, which protected to some extent the surface from further abrasion. Adding BN600 to the oil, a surface with delamination, tribofilms, furrows, and cracks was observed. A similar behaviour occurred adding MN500 (Figure 11(h,h1)) and MN600 (Figure 11(i,i1)). The disc surface was covered by shallow furrows, delamination, and wear debris together with tribofilm. The main mechanism in this case was abrasive wear due to the abrasion caused by the preferential pyramid particles shape which acted as a plough over the steel.

#### 4. Conclusions

This study investigated the effect of different types of polyphenolic extracts obtained from wine processing waste (whole pomace of Barbera variety and Moscato variety) on the size and shape of zinc oxide particles, analysing how their morphological and structural features influenced the tribological properties when added to a lubricant oil. The main conclusions drawn from the experiments are as follows.

- Moscato extracts were richer in polyphenolic compounds than Barbera ones, likely due to the different winemaking technology and the natural distribution of the molecules in the berry. Barbera GP extracts contained anthocyanins, HCTA, and flavonols, while Moscato seeds extracts lacked these compounds. Barbera tannins had lower mDP, gallate subunits, and different proportions of (+)-catechin and (–)-epicatechin. FTIR analysis showed similar absorption bands for the two extracts, with slight differences mainly related to the presence of fatty acids and their glycerides in seeds extract;
- XRD analysis revealed that all the ZnO particles had a hexagonal structure with space group symmetry P63mc. The lattice parameters of ZnO particles were close to standard values, except for those obtained from Moscato seed extract and zinc acetate synthesized at 600 °C (MA600), which had higher values. Crystallite size increased with synthesis temperature, particularly in the case of BN500. Nitrate-based ZnO had higher crystallite size than acetate-based one. The 100/002 intensity ratio showed that the ZnO synthesised with Moscato seed extract led to a lower ratio than that synthesised with Barbera GP, indicating preferential growth along the c-axis;
- The precursor significantly affected size and shape of the ZnO particles. Indeed, particles obtained from nitrate were bipyramidal-shaped, with copresence of spherical

nanoparticles when using Moscato, and around 10 to 20 microns in size, whereas those from acetate were quasi-spherical and between 50 and 200 nm in size;

- Regarding tribological results, the addition to oil of both nitrate and acetate-derived ZnO particles stabilized the friction coefficient. COF was slightly higher than the base oil for most sliding tests, particularly when MA600 was added to the oil. Less pronounced differences with other samples were observed. All the ZnO particles, except MA600 and MN600, improved the wear resistance compared to the standard oil. This behaviour appeared dependent on the morphological characteristics of the ZnO powders. Indeed, spherical nanoparticles, obtained using acetate, functioned both as ball bearings between friction surfaces and as fillers of the holes/defects created in the steel disc, inducing a repairing effect, then lowering the wear. In the case of microparticles, obtained from the nitrate salt, they functioned only as load bearing, being too big for acting as fillers. Indeed, the wear resistance of ZnO microparticles appeared lower if compared to ZnO nanoparticles. Furthermore, an uneven tribofilm was observed to develop.

Exploring different methods of polyphenol extraction and fractionation, the interaction between these extracts with diverse metal precursors, and fine-tuning of the synthesis conditions could lead to a highly efficient method of ZnO particle synthesis for defined industrial purposes. These research pathways are currently being investigated by our group.

**Author Contributions:** Conceptualization, G.G.d.C., M.G.F. and M.D.M.; methodology, G.G.d.C., M.G.F. and M.D.M.; investigation, G.G.d.C., M.G.F., M.D.M., S.M. and M.G.; data curation, G.G.d.C., M.G.F., M.D.M., S.M. and M.G.; writing—original draft preparation, G.G.d.C. and M.D.M.; writing—review and editing, G.G.d.C., M.G.F., M.D.M., S.M., E.M. and M.G. All authors have read and agreed to the published version of the manuscript.

**Funding:** The work has been partly supported by the European Union in the frame of MSCA Staff Exchanges Program, Project PHENOCYCLES grant number 101131420.

**Institutional Review Board Statement:** Not applicable.

**Informed Consent Statement:** Not applicable.

**Data Availability Statement:** The main data have been presented in the form of figures and tables.

**Conflicts of Interest:** The authors declare no conflicts of interest.

## References

1. Mirabella, N.; Castellani, V.; Sala, S. Current Options for the Valorization of Food Manufacturing Waste: A Review. *J. Clean. Prod.* **2014**, *65*, 28–41. [[CrossRef](#)]
2. Brandão, A.S.; Gonçalves, A.; Santos, J.M.R.C.A. Circular Bioeconomy Strategies: From Scientific Research to Commercially Viable Products. *J. Clean. Prod.* **2021**, *295*, 126407. [[CrossRef](#)]
3. Makris, D.P.; Boskou, G.; Andrikopoulos, N.K. Polyphenolic Content and in Vitro Antioxidant Characteristics of Wine Industry and Other Agri-Food Solid Waste Extracts. *J. Food Compos. Anal.* **2007**, *20*, 125–132. [[CrossRef](#)]
4. Muhlack, R.A.; Potumarthi, R.; Jeffery, D.W. Sustainable Wineries through Waste Valorisation: A Review of Grape Marc Utilisation for Value-Added Products. *Waste Manag.* **2018**, *72*, 99–118. [[CrossRef](#)] [[PubMed](#)]
5. Verma, R.; Pathak, S.; Srivastava, A.K.; Praver, S.; Tomljenovic-Hanic, S. ZnO Nanomaterials: Green Synthesis, Toxicity Evaluation and New Insights in Biomedical Applications. *J. Alloys Compd.* **2021**, *876*, 160175. [[CrossRef](#)]
6. Kumar, J.A.; Krithiga, T.; Manigandan, S.; Sathish, S.; Renita, A.A.; Prakash, P.; Prasad, B.S.N.; Kumar, T.R.P.; Rajasimman, M.; Hosseini-Bandegharai, A.; et al. A Focus to Green Synthesis of Metal/Metal Based Oxide Nanoparticles: Various Mechanisms and Applications towards Ecological Approach. *J. Clean. Prod.* **2021**, *324*, 129198. [[CrossRef](#)]
7. Ijaz, I.; Bukhari, A.; Gilani, E.; Nazir, A.; Zain, H.; Saeed, R.; Hussain, S.; Hussain, T.; Bukhari, A.; Naseer, Y.; et al. Green Synthesis of Silver Nanoparticles Using Different Plants Parts and Biological Organisms, Characterization and Antibacterial Activity. *Environ. Nanotechnol. Monit. Manag.* **2022**, *18*, 100704. [[CrossRef](#)]
8. Xia, C.; Jin, X.; Garalleh, H.A.; Garaleh, M.; Wu, Y.; Hill, J.M.; Pugazhendhi, A. Optimistic and Possible Contribution of Nanomaterial on Biomedical Applications: A Review. *Environ. Res.* **2023**, *218*, 114921. [[CrossRef](#)]
9. Cui, Y.; Ding, M.; Sui, T.; Zheng, W.; Qiao, G.; Yan, S.; Liu, X. Role of Nanoparticle Materials as Water-Based Lubricant Additives for Ceramics. *Tribol. Int.* **2020**, *142*, 105978. [[CrossRef](#)]

10. Ouyang, T.; Tang, W.; Pan, M.; Tang, J.; Huang, H. Friction-Reducing and Anti-Wear Properties of 3D Hierarchical Porous Graphene/Multi-Walled Carbon Nanotube in Castor Oil under Severe Condition: Experimental Investigation and Mechanism Study. *Wear* **2022**, *498–499*, 204302. [[CrossRef](#)]
11. Alves, S.M.; Mello, V.S.; Faria, E.A.; Camargo, A.P.P. Nanolubricants Developed from Tiny CuO Nanoparticles. *Tribol. Int.* **2016**, *100*, 263–271. [[CrossRef](#)]
12. Dai, W.; Kheireddin, B.; Gao, H.; Liang, H. Roles of Nanoparticles in Oil Lubrication. *Tribol. Int.* **2016**, *102*, 88–98. [[CrossRef](#)]
13. Waqas, M.; Zahid, R.; Bhutta, M.U.; Khan, Z.A.; Saeed, A. A Review of Friction Performance of Lubricants with Nano Additives. *Materials* **2021**, *14*, 6310. [[CrossRef](#)] [[PubMed](#)]
14. Wu, Y.Y.; Tsui, W.C.; Liu, T.C. Experimental Analysis of Tribological Properties of Lubricating Oils with Nanoparticle Additives. *Wear* **2007**, *262*, 819–825. [[CrossRef](#)]
15. Mousavi, S.B.; Heris, S.Z.; Estellé, P. Experimental Comparison between ZnO and MoS<sub>2</sub> Nanoparticles as Additives on Performance of Diesel Oil-Based Nano Lubricant. *Sci. Rep.* **2020**, *10*, 5813. [[CrossRef](#)] [[PubMed](#)]
16. Bhaumik, S.; Maggirwar, R.; Datta, S.; Pathak, S.D. Analyses of Anti-Wear and Extreme Pressure Properties of Castor Oil with Zinc Oxide Nano Friction Modifiers. *Appl. Surf. Sci.* **2018**, *449*, 277–286. [[CrossRef](#)]
17. Hernandez Battez, A.; Fernandez Rico, J.E.; Navas Arias, A.; Viesca Rodriguez, J.L.; Chou Rodriguez, R.; Diaz Fernandez, J.M. The Tribological Behaviour of ZnO Nanoparticles as an Additive to PAO6. *Wear* **2006**, *261*, 256–263. [[CrossRef](#)]
18. Arumugam, S.; Baskar, S.; Sankaranarayanan, S.; Athreya, S.H.; Narayanan, N.L.; Prasad, S.S.D. Influence of Morphology of Anti-Wear Nano Additives on Tribological Behavior of Chemically Modified Rapeseed Oil. *IOP Conf. Ser. Mater. Sci. Eng.* **2018**, *390*, 012017. [[CrossRef](#)]
19. Guaita, M.; Panero, L.; Motta, S.; Mangione, B.; Bosso, A. Effects of High-Temperature Drying on the Polyphenolic Composition of Skins and Seeds from Red Grape Pomace. *LWT* **2021**, *145*, 111323. [[CrossRef](#)]
20. Kennedy, J.A.; Jones, G.P. Analysis of Proanthocyanidin Cleavage Products Following Acid-Catalysis in the Presence of Excess Phloroglucinol. *J. Agric. Food Chem.* **2001**, *49*, 1740–1746. [[CrossRef](#)]
21. Bosso, A.; Cassino, C.; Motta, S.; Panero, L.; Tsolakis, C.; Guaita, M. Polyphenolic Composition and In Vitro Antioxidant Activity of Red Grape Seeds as Byproducts of Short and Medium-Long Fermentative Macerations. *Foods* **2020**, *9*, 1451. [[CrossRef](#)] [[PubMed](#)]
22. Ummano, I.; Ferrandino, A.; Di Stefano, R.; Cravero, M.C. Evoluzione Dei Polifenoli Di Uve Di Biotipi Di Pinot Nero Durante La Maturazione. *L'Enologo* **2001**, *XXXVII*, 71–82.
23. Motta, S.; Guaita, M.; Petrozziello, M.; Panero, L.; Bosso, A. Effect of Reductive Pressing on the Concentration of Reduced Glutathione and Phenols in the Musts of Four Italian Cultivars. *Am. J. Enol. Vitic.* **2014**, *65*, 471–478. [[CrossRef](#)]
24. Di Stefano, R.; Cravero, M.C. Metodi per Lo Studio Dei Polifenoli Dell'uva. *Riv. Vitic. Enol.* **1991**, *2*, 37–45.
25. Zum Gahr, K.-H.; Wahl, R.; Wauthier, K. Experimental Study of the Effect of Microtexturing on Oil Lubricated Ceramic/Steel Friction Pairs. *Wear* **2009**, *267*, 1241–1251. [[CrossRef](#)]
26. Guaita, M.; Motta, S.; Messina, S.; Casini, F.; Bosso, A. Polyphenolic Profile and Antioxidant Activity of Green Extracts from Grape Pomace Skins and Seeds of Italian Cultivars. *Foods* **2023**, *12*, 3880. [[CrossRef](#)] [[PubMed](#)]
27. Lucarini, M.; Durazzo, A.; Kiefer, J.; Santini, A.; Lombardi-Boccia, G.; Souto, E.B.; Romani, A.; Lampe, A.; Ferrari Nicoli, S.; Gabrielli, P.; et al. Grape Seeds: Chromatographic Profile of Fatty Acids and Phenolic Compounds and Qualitative Analysis by FTIR-ATR Spectroscopy. *Foods* **2020**, *9*, 10. [[CrossRef](#)] [[PubMed](#)]
28. Varasteh, M.; Deng, Z.; Hwang, H.; Kim, Y.J.; Wong, G.B. Quantitative Determination of Polymorphic Impurity by X-ray Powder Diffractometry in an OROS<sup>®</sup> Formulation. *Int. J. Pharm.* **2009**, *366*, 74–81. [[CrossRef](#)] [[PubMed](#)]
29. Gautier di Confienzo, G.; Faga, M.G.; La Parola, V.; Magnacca, G.; Paganini, M.C.; Testa, M.L. Microwave Approach and Thermal Decomposition: A Sustainable Way to Produce ZnO Nanoparticles with Different Chemo-Physical Properties. *Mater. Chem. Phys.* **2024**, *321*, 129485. [[CrossRef](#)]
30. McLaren, A.; Valdes-Solis, T.; Li, G.; Tsang, S.C. Shape and Size Effects of ZnO Nanocrystals on Photocatalytic Activity. *J. Am. Chem. Soc.* **2009**, *131*, 12540–12541. [[CrossRef](#)]
31. Dutta, S.; Chattopadhyay, S.; Sarkar, A.; Chakrabarti, M.; Sanyal, D.; Jana, D. Role of Defects in Tailoring Structural, Electrical and Optical Properties of ZnO. *Prog. Mater. Sci.* **2009**, *54*, 89–136. [[CrossRef](#)]
32. Goswami, M.; Adhikary, N.C.; Bhattacharjee, S. Effect of Annealing Temperatures on the Structural and Optical Properties of Zinc Oxide Nanoparticles Prepared by Chemical Precipitation Method. *Optik* **2018**, *158*, 1006–1015. [[CrossRef](#)]
33. Chen, Y.; Jyoti, N.; Hyun-U, K.; Kim, J. Effect of Annealing Temperature on the Characteristics of ZnO Thin Films. *J. Phys. Chem. Solids* **2012**, *73*, 1259–1263. [[CrossRef](#)]
34. Perez-Lopez, O.W.; Farias, A.C.; Marcilio, N.R.; Bueno, J.M.C. The Catalytic Behavior of Zinc Oxide Prepared from Various Precursors and by Different Methods. *Mater. Res. Bull.* **2005**, *40*, 2089–2099. [[CrossRef](#)]
35. Sherin, L.; Sohail, A.; Amjad, U.-S.; Mustafa, M.; Jabeen, R.; Ul-Hamid, A. Facile Green Synthesis of Silver Nanoparticles Using Terminalia Bellerica Kernel Extract for Catalytic Reduction of Anthropogenic Water Pollutants. *Colloid. Interface Sci. Commun.* **2020**, *37*, 100276. [[CrossRef](#)]
36. Naseer, M.; Aslam, U.; Khalid, B.; Chen, B. Green Route to Synthesize Zinc Oxide Nanoparticles Using Leaf Extracts of Cassia Fistula and Melia Azadarach and Their Antibacterial Potential. *Sci. Rep.* **2020**, *10*, 9055. [[CrossRef](#)] [[PubMed](#)]

37. Nava, O.J.; Soto-Robles, C.A.; Gómez-Gutiérrez, C.M.; Vilchis-Nestor, A.R.; Castro-Beltrán, A.; Olivas, A.; Luque, P.A. Fruit Peel Extract Mediated Green Synthesis of Zinc Oxide Nanoparticles. *J. Mol. Struct.* **2017**, *1147*, 1–6. [[CrossRef](#)]
38. Bandeira, M.; Possan, A.L.; Pavin, S.S.; Raota, C.S.; Vebber, M.C.; Giovanela, M.; Roesch-Ely, M.; Devine, D.M.; Crespo, J.S. Mechanism of Formation, Characterization and Cytotoxicity of Green Synthesized Zinc Oxide Nanoparticles Obtained from *Ilex Paraguariensis* Leaves Extract. *Nano-Struct. Nano-Objects* **2020**, *24*, 100532. [[CrossRef](#)]
39. Han, X.; Thrush, S.J.; Zhang, Z.; Barber, G.C.; Qu, H. Tribological Characterization of ZnO Nanofluids as Fastener Lubricants. *Wear* **2021**, *468–469*, 203592. [[CrossRef](#)]
40. Wang, B.; Qiu, F.; Barber, G.C.; Zou, Q.; Wang, J.; Guo, S.; Yuan, Y.; Jiang, Q. Role of Nano-Sized Materials as Lubricant Additives in Friction and Wear Reduction: A Review. *Wear* **2022**, *490–491*, 204206. [[CrossRef](#)]
41. Liu, G.; Li, X.; Qin, B.; Xing, D.; Guo, Y.; Fan, R. Investigation of the Mending Effect and Mechanism of Copper Nano-Particles on a Tribologically Stressed Surface. *Tribol. Lett.* **2004**, *17*, 961–966. [[CrossRef](#)]
42. Ali, M.K.A.; Xianjun, H.; Mai, L.; Qingping, C.; Turkson, R.F.; Bicheng, C. Improving the Tribological Characteristics of Piston Ring Assembly in Automotive Engines Using Al<sub>2</sub>O<sub>3</sub> and TiO<sub>2</sub> Nanomaterials as Nano-Lubricant Additives. *Tribol. Int.* **2016**, *103*, 540–554. [[CrossRef](#)]
43. Wang, Y.; Zhang, L.; Liu, A.; Wu, C.; Li, W. Tribological Performance of Silicone Oil Based Al<sub>2</sub>O<sub>3</sub> Nano Lubricant for an Mg Alloy Subjected to Sliding at Elevated Temperatures. *Tribol. Int.* **2022**, *175*, 107779. [[CrossRef](#)]

**Disclaimer/Publisher’s Note:** The statements, opinions and data contained in all publications are solely those of the individual author(s) and contributor(s) and not of MDPI and/or the editor(s). MDPI and/or the editor(s) disclaim responsibility for any injury to people or property resulting from any ideas, methods, instructions or products referred to in the content.